1-1-1997

SPIRIT III Radiometer Saturation Effect

Joseph J. Tansock

Tansock, Joseph J. 1997. "SPIRIT III Radiometer Saturation Effect." Optical Engineering, 36 (11): 2963–70. doi:10.1117/1.601537.

SPIRIT III radiometer saturation effect

Joseph J. Tansock, MEMBER SPIE
Utah State University
Space Dynamics Laboratory
1695 North Research Park Way
North Logan, Utah 84341
E-mail: joe.tansock@sdl.usu.edu

Abstract. The Space Dynamics Laboratory at Utah State University (SDL/USU) calibrated the spatial infrared imaging telescope (SPIRIT) radiometer as part of its contract with the Ballistic Missile Defense Organization (BMDO). During the calibration effort, SDL/USU discovered and characterized a phenomenon that reduces the detector dark offset and responsivity after saturation, which results in increased calibration uncertainties directly following a saturation event. The magnitude and recovery duration for the dark offset and responsivity depend on several variables, including saturation flux level, saturation integration mode, integration mode, focal plane temperature, and saturation duration. Detector-to-detector variations in the magnitude of the saturation effect were also observed for detectors within an array. This phenomenon and the methods used to characterize it are described. [S0091-3286(97)00411-X]

Subject terms: infrared radiometric sensor calibration; saturation; dark offset; responsivity; infrared sensor; blocked impurity band detectors.

Paper RSC-04 received May 15, 1997; revised manuscript received July 2, 1997; accepted for publication July 10, 1997.

1 Introduction

The Space Dynamics Laboratory at Utah State University (SDL/USU) designed, built, and calibrated the spatial infrared imaging telescope (SPIRIT III) sensor as part of the Midcourse Space Experiment (MSX), sponsored by the Ballistic Missile Defense Organization (BMDO). MSX was successfully launched on April 24, 1996 and has been fulfilling its mission objectives since that time.

SDL/USU calibrated the SPIRIT III radiometer in several ground calibration efforts and continues to upgrade the calibration with on-orbit measurements. As part of the radiometer ground calibration, SDL/USU discovered and characterized a saturation phenomenon termed the radiometer saturation effect.[1] This effect causes a temporary reduction in detector dark offset and responsivity, resulting in increased calibration uncertainties directly following a saturation event.

The dark offset is the mean response to 0 input flux. It is unique for each detector and is dependent on focal plane temperature and time from power-up. The focal plane temperature was controlled with a heater and the instrument was allowed to stabilize after turn-on. The long-term stability of the dark offset for these conditions is documented[2] and ranges from 0.2 counts to 2 counts, depending on the array and integration mode.

The magnitude and recovery duration for the dark offset and responsivity depend on several variables, including saturation flux level, saturation integration mode, integration mode, focal plane temperature, and saturation duration. Detector-to-detector variations in the magnitude of the saturation effect were also observed for detectors within an array. This paper describes this phenomenon and the methods used to characterize it.

The results of the saturation effect characterization were used for on-orbit experiment planning and for quantifying measurement uncertainties following a saturation event.

1.1 *Radiometer Description*

The SPIRIT III radiometer consists of a cryogenically cooled high off-axis rejection telescope, scan mirror, spectral beamsplitters and filters, and five focal plane detector modules.[3] The five focal plane modules are designated as A through E. Focal plane modules A and B were designed and manufactured by Aerojet Electrosystems Company, and modules C, D, and E were designed and manufactured by Rockwell International. Each detector array is spectrally filtered to a unique passband between 4 and 28 μm. Each radiometer focal plane array consists of 192 rows and 8 columns of impurity band conductor, blocked impurity band (IBC/BIB) arsenic-doped silicon detectors mounted to a field-effect transistor (FET), low-noise, cryogenic readout circuits.

The scan mirror can scan or stop in either of the radiometer's two modes of operation: mirror-scan mode or earthlimb mode. Three selectable integration modes are available in the mirror-scan mode, and four selectable integration modes are available in the earthlimb (EL) mode. The mirror-scan (MS) integration modes are designated MS1, MS4, and MS4+, and have integration times of approximately 2.8, 0.69, and 0.17 ms. The earthlimb integration modes are EL1, EL4, EL16, and EL16+, and have integration times of approximately 14, 3.5, 0.87, and 0.22 ms.

2 Radiometer Saturation Effect

The radiometer saturation effect discovered during the SPIRIT III radiometer calibration resulted in a reduced detector dark offset and responsivity immediately after a saturation event. The dark offset and responsivity exponentially recovered to nominal values within about 30 min. Further testing was performed to better understand both the saturation effect on the dark offset and responsivity. Data were

collected in one of two data collection sequences: saturation/dark offset, or saturation/response. The saturation/dark offset sequence measured 100 minor frames of the radiometer's dark offset before and periodically after saturation for 25 min. An external blackbody was used along with the calibrator configured for its collimated source as the saturation source. The saturation/response sequence measured 100 minor frames of the radiometer's response to various sources before and periodically after saturation for 25 min. Unless specified, the radiometer shutter stimulators were disabled, the saturation duration was approximately 13 s, and the focal plane temperature was approximately 10 K.

2.1 *Saturation Dark Offset Effect*

The saturation dark offset effect was evaluated using data from the saturation/dark offset and saturation/response data collection sequences. Equation (1) was used to calculate the dark offset difference as a function of time from saturation.

$$\mathrm{DO}_{\mathrm{diff}}(t) = \mathrm{DO}(t) - \mathrm{DO}_{\mathrm{nominal}}, \tag{1}$$

where $\mathrm{DO}_{\mathrm{diff}}(\ )$ is the dark offset difference (in counts), $\mathrm{DO}(\ )$ is the dark offset (in counts), $\mathrm{DO}_{\mathrm{nominal}}$ is the nominal dark offset (in counts), and t is the time from saturation (in minutes).

To reduce noise in the estimated dark offset, 100 minor frames of dark offset data from those detectors that were directly saturated were averaged. To quantify the amplitude and recovery time constant of the saturation dark offset effect, Eq. (2) was used to curve fit the dark offset difference as a function of time from saturation:

$$\mathrm{DO}_{\mathrm{diff}}(t) = (\mathrm{AMP})\exp\left(-\frac{t}{\tau}\right) + c, \tag{2}$$

where $\mathrm{DO}_{\mathrm{diff}}(\ )$ is the dark offset difference (in counts), AMP is the amplitude curve fit coefficient (in counts), τ is the recovery time constant curve fit coefficient (in minutes), and c is the constant curve fit coefficient (in counts).

Depending on the array, complete recovery from the saturation dark offset effect did not occur by the end of the data collection sequence. This results in a residual dark offset at the beginning of the next data collection sequence. The constant term shown in Eq. (2) was included in the curve fit to account for this residual dark offset.

2.2 *Saturation Responsivity Effect*

The saturation responsivity effect was evaluated using data from the saturation/response data collection sequence. Equation (3) was used to calculate the percent response difference to the second-generation multifunction IR calibrator (MIC2) scatter source as a function of time from saturation.

$$\mathrm{Resp}_{\mathrm{diff}}(t) = \frac{\mathrm{Resp}(t) - \mathrm{Resp}_{\mathrm{nominal}}}{\mathrm{Resp}_{\mathrm{nominal}}} \times 100, \tag{3}$$

where $\mathrm{Resp}_{\mathrm{diff}}(\ )$ is the response difference to the MIC2 scatter source (in percent), $\mathrm{Resp}(\ )$ is the offset corrected response to the MIC2 scatter source (in counts), $\mathrm{Resp}_{\mathrm{nominal}}$ is the nominal offset corrected response to the MIC2 scatter source (in counts), and t is the time from saturation (in minutes).

To reduce noise in the estimated response, 100 minor frames of response data from those detectors that were directly saturated were averaged.

To quantify the amplitude and recovery time constant of the saturation responsivity effect, Eq. (4) was used to curve fit the response percentage difference as a function of time from saturation.

$$\mathrm{Resp}_{\mathrm{diff}}(t) = (\mathrm{AMP})\exp\left(-\frac{t}{\tau}\right), \tag{4}$$

where $\mathrm{Resp}_{\mathrm{diff}}(\ )$ is the response difference (in percent), AMP is the amplitude curve fit coefficient (in counts), and τ is the recovery time constant curve fit coefficient (in minutes).

A constant curve fit coefficient was not needed in Eq. (4) because the data showed complete recovery of the saturation responsivity effect within the data collection sequence.

3 Results and Discussion

The saturation dark offset effect and saturation responsivity effect were evaluated as a function of saturation flux level, saturation integration mode, integration mode, focal plane temperature, and detector-to-detector variations.

Figures 1 and 2 show representative curves for the saturation dark offset effect and saturation responsivity effect, respectively, for all arrays for different saturation flux levels. The saturation flux levels are expressed as a saturation factor multiplied by the saturation equivalent radiance (SER). At saturation, the SER is equal to 1. These figures show that all arrays experienced the saturation effect, regardless of manufacturer. The saturation effect was array dependent, however, and all arrays have different magnitudes and recovery durations. The figures also show that the dark offset and responsivity exponentially recovered to nominal values within about 30 min.

To describe the saturation effect as a function of the various parameters studied in this paper, figures are shown only for the array that best illustrates the saturation effect, although results from other arrays are discussed. Complete results for all arrays and data sets have been documented.[4]

3.1 *Saturation Flux Level*

The saturation dark offset and saturation responsivity effects were evaluated as a function of saturation flux level. The differences in dark offset and responsivity were first plotted versus time from saturation for each array (Figs. 1 and 2). Curves were then fit to these data using Eqs. (2) and (4). Figure 3 shows the curve fit amplitudes as a function of saturation flux level for the saturation dark offset effect for array C, a typical array. The saturation flux levels are expressed as a saturation factor multiplied by the SER. At saturation, the SER is equal to 1. Figure 3 shows that the amplitude of the saturation dark offset effect increased to an array-dependent saturation flux level, and then decreased slightly for larger saturation flux levels. Most of the arrays showed this general effect, although the slight decrease in amplitude at larger saturation flux levels was not apparent

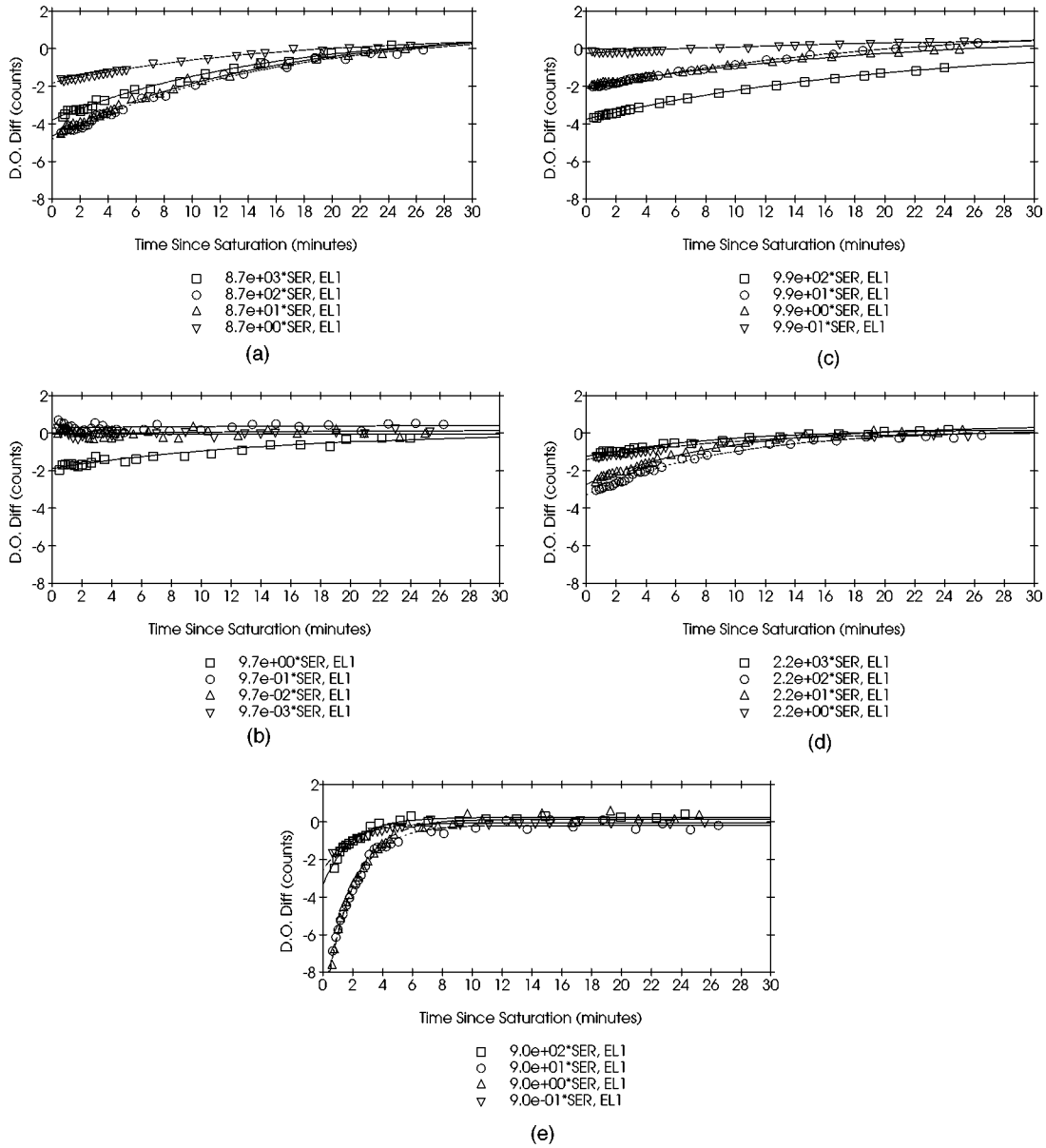

Fig. 1 Saturation dark offset effect for different saturation flux levels for arrays (a) A (EL1), (b) B2 (EL1), (c) C (EL1), (d) D (EL1), and (e) E (EL1).

in all arrays. The maximum dark offset amplitudes ranged from -4 to -10 counts at SERs ranging from 10 to 500.

The saturation dark offset data include data for which no stimulus was presented to the arrays after saturation, and data for which the arrays were periodically stimulated after saturation with the calibrator's scatter source and internal shutter stimulators. Figure 3 shows the amplitude of the saturation effects to be independent of array stimulus, which was true for all arrays.

Figure 4 shows the curve fit amplitudes as a function of saturation flux level for array C's saturation responsivity effect. As with the dark offset effect, this figure shows that the amplitude of the saturation responsivity effect increased to an array-dependent saturation flux level, and then remained the same or decreased slightly for larger saturation flux levels. The maximum amplitude of the saturation responsivity effect ranged from about -14 to -3% for SERs equal to 10 to 500. Several arrays showed a measurable saturation responsivity effect for saturation flux levels that were at or slightly less than saturation.

The saturation responsivity data included data in which the arrays were periodically stimulated by the calibration chamber scatter source as well as the shutter stimulators. Figure 4 shows the amplitude of the saturation responsivity effects is also independent of array stimulus, and was true for all arrays.

Although the time required for the arrays to recover from the saturation effects does not depend on the saturation flux level, each array does have its own recovery time, which is dependent on stimulus received after saturation. The recovery time constant for each array was determined from the average of the curve fit coefficients. Table 1

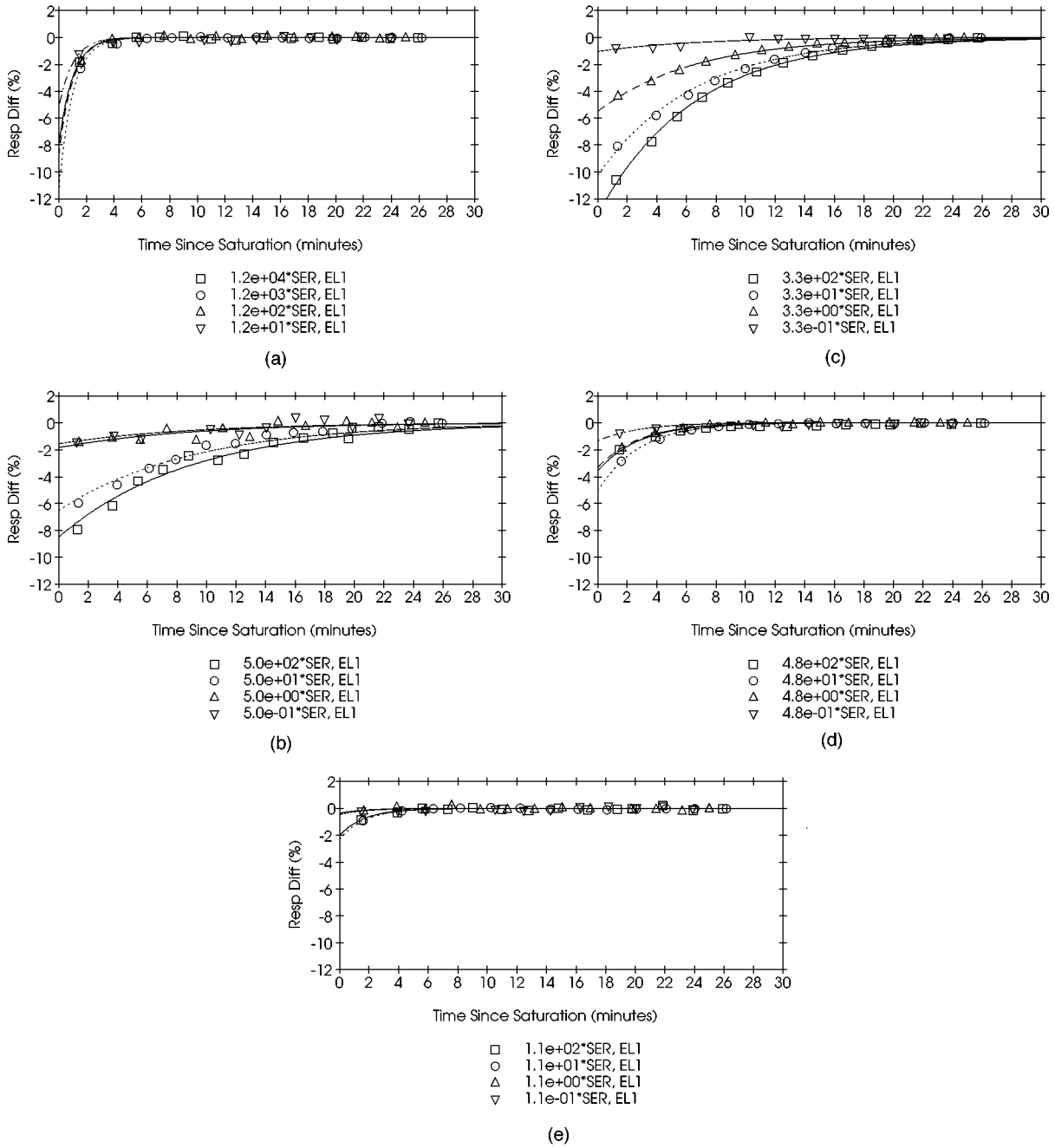

Fig. 2 Saturation responsivity effect for different saturation flux levels (shutter stims disabled) for arrays (a) A (EL4), (b) B2 (EL1), (c) C (EL1), (d) D (EL1), and (e) E (EL1).

shows the recovery time constant for each array as a function of array stimulus. These data show that, with one exception, the recovery time constants for both the saturation dark offset effect and the saturation responsivity effect were reduced (i.e., quicker recovery) by stimulating the arrays. For the responsivity effect array A had a short recovery time constant (about 1 min) and was independent of stimulation.

Table 1 also shows that the recovery time constants are similar for the dark offset effect and the responsivity effect for the same external stimulation. Although the saturation responsivity effect could not be measured without some external stimulation, this comparison suggests that the saturation responsivity effect recovery time constant with no external stimulation would be much larger, as observed in the dark offset effect recovery time constants.

3.2 *Saturation Integration Mode*

To determine if placing an array in a lower gain (shorter integration time) protects the arrays from the radiometer saturation effect, the dark offset and responsivity differ-

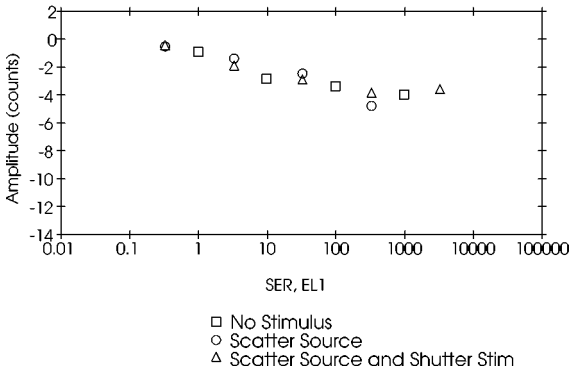

Fig. 3 Saturation dark offset effect amplitude for different saturation flux levels (amplitude versus saturation flux levels).

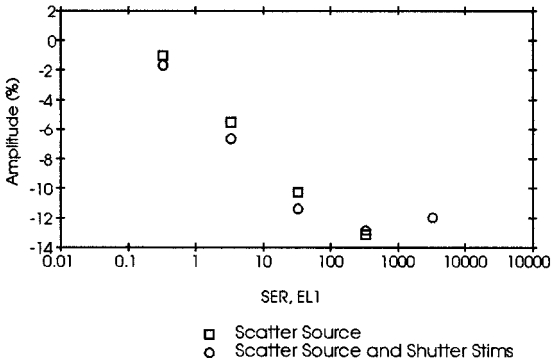

Fig. 4 Saturation responsivity effect amplitude for different saturation flux levels.

ences for the EL1 integration mode were plotted versus time from saturation for different saturation integration mode settings. Figures 5 and 6 show the normalized curve fit amplitudes as functions of integration times for array C. These figures show that placing the array in a lower gain during saturation does provide some shielding from the saturation effect. For example, placing the arrays in low gain [EL16+(0.2 ms) or MS4+(0.17 ms)] rather than high gain [EL1 (14 ms)] during saturation reduced the saturation dark offset amplitude by a factor of 2 for array C, with reductions ranging from a factor of 2 to 10 for the other arrays. The saturation responsivity effect amplitude was also reduced by a factor of 2 for array C, and varied by a factor of 2 to 5 for the other arrays. Although a reduction occurs, the saturation effect is not completely eliminated by this technique, even though the detectors may not saturate while observing the bright source in the lower gain.

3.3 *Integration Mode*

The saturation dark offset effect was evaluated as a function of integration mode by plotting the dark offset difference versus time from saturation for different integration mode settings and different data collection sequences. All arrays were saturated in the EL1 integration mode. Figure 7 shows the normalized amplitude of the curve fit coefficients as a function of integration time for array D. This figure is typical of other arrays and shows that the amplitude of the saturation dark offset effect approximately scales with integration time.

The saturation responsivity effect as a function of integration mode was evaluated by comparing the array's response to the calibration chamber scatter source with the response to the shutter stimulators. The percentage response difference versus time from saturation for these data are shown in Fig. 8 for array C. The curve fits show that the amplitude of the saturation dark offset effect is similar for the EL1 and EL4 integration modes, giving evidence that the saturation responsivity effect is independent of integration time.

3.4 *Focal Plane Temperature*

The saturation dark offset and saturation responsivity effects as a function of focal plane temperature were evaluated by first plotting the dark offset and responsivity differences versus time from saturation for different focal plane temperatures. Curves were then fit to the data. Figure 9 shows the curve fit amplitudes versus thermal link temperature for array B, and Fig. 10 shows the saturation dark offset effect curve fit recovery time constants for array B. Figure 9 is typical of other arrays and shows that the amplitude of the saturation dark offset effect increases with increasing temperature. In general, the amplitude is small and similar among arrays for focal plane temperatures of 9.0 and 10.0 K, but increases for higher temperatures, ranging from -6 to -90 counts for 11.0 and 12.0 K, depending on the array.

Figure 10 shows two recovery time constant dependencies. First, the recovery time constant is shortened when the

Table 1 Saturation/dark offset effect and saturation/response effect recovery time constants (focal plane temperature=10.13 K).

		Recovery Time Constant (minutes)				
Saturation Effect	External Stimulus	Array A	Array B	Array C	Array D	Array E
Dark offset	None	14.9	15.0	20.5	9.0	1.9
	Calibrator scatter source	1.0	12.1	9.2	2.8	1.7
	Calibrator scatter source and shutter stimulators	1.2	4.1	4.7	2.3	1.6
Responsivity	None	—	—	—	—	—
	Calibrator scatter source	1.0	9.0	6.5	2.8	1.7
	Calibrator scatter source and shutter stimulators	1.2	4.1	3.8	2.1	1.6

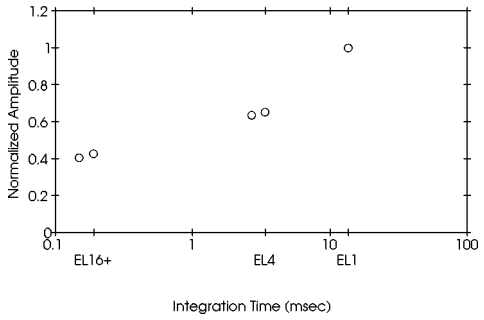

Fig. 5 Saturation dark offset effect amplitude versus saturation integration time.

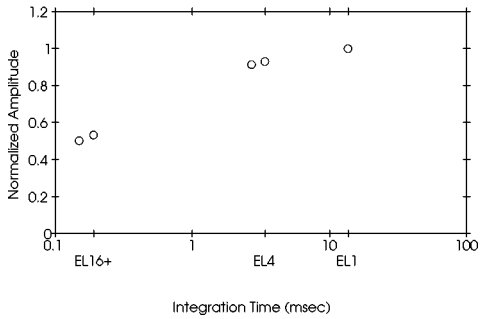

Fig. 6 Saturation responsivity effect amplitude versus saturation integration time.

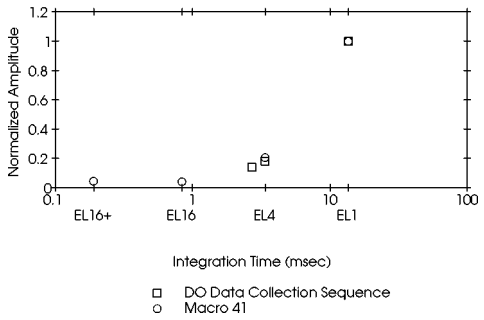

Fig. 7 Saturation dark offset effect for different integration modes (amplitude versus integration time).

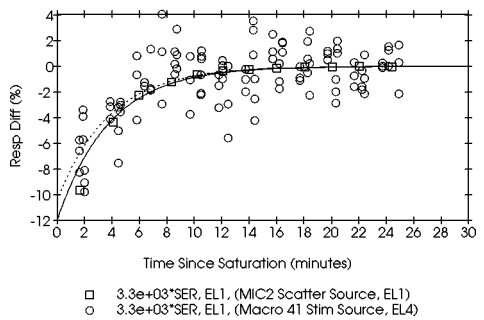

Fig. 8 Saturation responsivity effect for different integration modes.

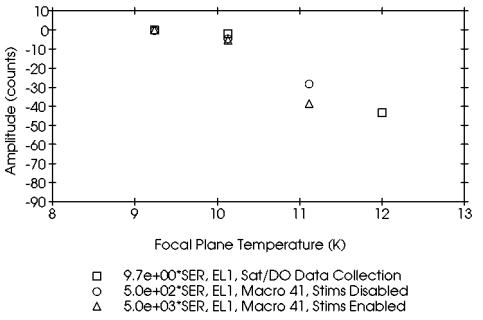

Fig. 9 Saturation dark offset effect amplitude versus focal plane temperature.

array is stimulated during data collection at 9.0 and 10.0 K (shutter stimulators disabled versus enabled). Second, the time constant becomes shorter for focal plane temperatures warmer than 10.0 K. In general, the recovery time constant is less than 3 min for focal plane temperatures above 11.0 K for all arrays.

The curve fit results for the saturation responsivity effect are shown in Figs. 11 and 12 for array C. In Fig. 11, the amplitude of the saturation responsivity effect remains at approximately the same value for focal plane temperatures between 9.0 and 11.0 K. The amplitude of the saturation responsivity effect for 12.0 K could not be quantified from a curve fit because responsivity recovery was reached before the first data point at approximately 1.8 min following saturation. Figure 12 shows the same recovery time constant dependencies as the saturation dark offset effect: the recovery time constant is shortened when the array is stimulated during data collection, and the time constant becomes shorter for warmer focal plane temperatures.

3.5 *Saturation Duration*

To determine the effect of saturation duration on the radiometer saturation effect, the dark offset and responsivity differences were plotted versus time from saturation for saturation durations of 15 ms, 46 ms, 13 s, and 3 min, and curves were fit to the data. The amplitudes of these curve fits for the saturation dark offset and responsivity effects for array D are shown in Figs. 13 and 14, respectively, as a function of saturation duration. The 15- and 46-ms saturations were accomplished by scanning a source over the array at appropriate velocities.

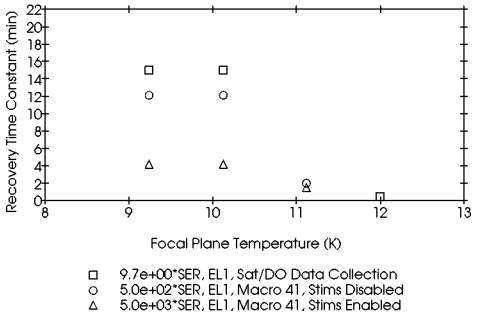

Fig. 10 Saturation dark offset effect recovery time constant versus focal plane temperature.

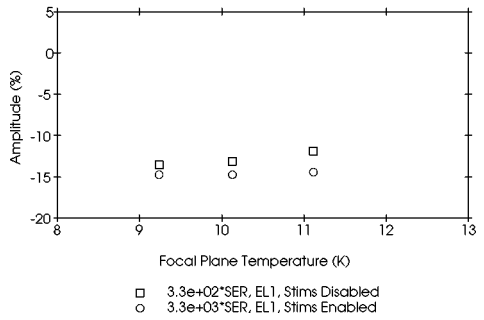

Fig. 11 Saturation responsivity effect amplitude versus focal plane temperature.

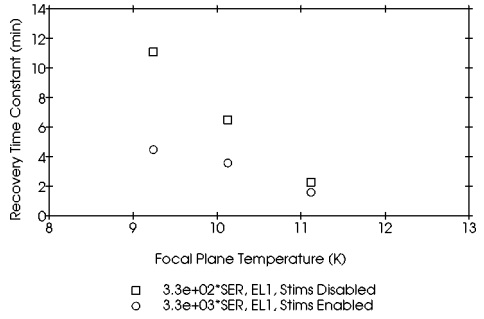

Fig. 12 Saturation responsivity effect recovery time constant versus focal plane temperature.

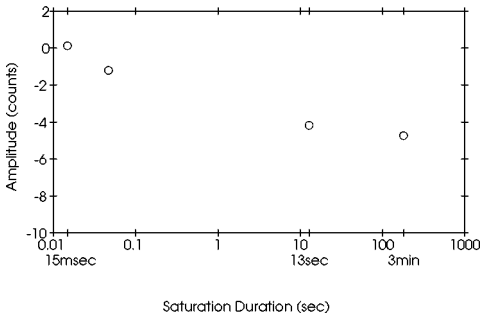

Fig. 13 Saturation dark offset effect amplitude versus saturation duration.

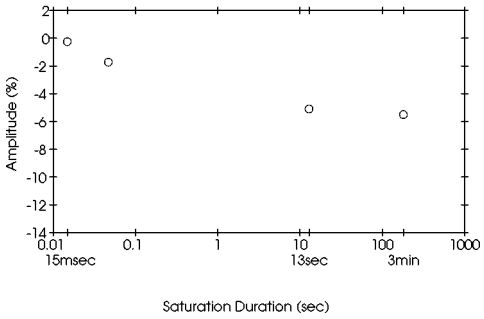

Fig. 14 Saturation responsivity effect amplitude versus saturation duration.

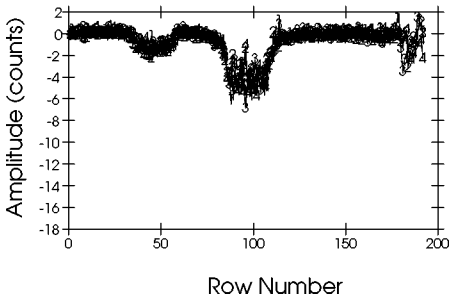

Fig. 15 Saturation dark offset effect amplitude for individual detectors.

In general, the amplitudes of the saturation dark offset and saturation responsivity effects were similar for the 13-s and 3-min saturations for all arrays. For the saturation dark offset effect, the amplitude of the effect for array D was about -4.5 counts, and ranged from -4.5 to nearly -10 counts among the arrays for these saturation durations. For the 15-ms saturation, which is equivalent to an array's point source scan, the amplitude for the saturation dark offset effect was nearly 0 counts for four of the five arrays.

For the saturation responsivity effect, the amplitude of the effect for the 13-s and 3-min saturation durations was about -5.5% for array D and ranged from -2 to nearly -13% among all arrays. For the 15-ms saturation, the amplitude for the saturation responsivity effect was nearly 0% for four of the five arrays. These results show the saturation effect remains unchanged for saturation durations greater than 13 s and is less for saturation durations less than 46 ms.

3.6 *Detector-to-Detector Variation*

The detector-to-detector variation of the saturation dark offset and responsivity effects was evaluated by performing a curve fit on each nominal detector within an array. Figures 15 and 16 are pixel plots showing the curve fit amplitudes as a function of detector row number for the saturation dark offset and saturation responsivity effects, respectively, using array D as an example. The EL1 integration mode was used to obtain the data in these figures.

Figures 15 and 16 clearly identify the detectors that were directly saturated and show that the saturation event saturated detectors near the center of the array. The nonzero amplitude of the saturation effects located to the left of center is due to an inadvertent saturation from the saturating source being passed over the array after being removed from array C. The saturation duration for these detectors is estimated to be approximately 46 ms, the time required for the source to move over the array. These data show that detectors that are not directly saturated are not affected by the saturation dark offset effect.

In general, the peak-to-peak variation of the saturation dark offset effect amplitude for those detectors that were directly saturated ranges from approximately 2 to nearly 10 counts among the arrays. The peak-to-peak variation of the saturation responsivity effect for those detectors that were directly saturated ranged from approximately 4 to nearly 10% among arrays.

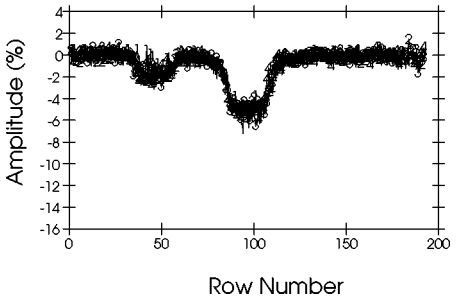

Fig. 16 Saturation responsivity effect amplitude for individual detectors.

4 Summary

The radiometer saturation effect was observed on all of the five arrays, regardless of manufacturer. The results of the radiometer saturation effect study showed that the magnitude of the saturation effect for both dark offset and responsivity is dependent on saturation flux level. The magnitude of this effect increases for increasing saturation flux levels up to an array-dependent saturation level, and then remains the same or decreases slightly for larger saturation flux levels. Placing an array in low gain during saturation provides some shielding from the saturation effect, but the saturation effect can occur as a result of viewing a bright source in a low-gain integration mode, even if the detectors do not actually saturate. The amplitude of the saturation dark offset effect is proportional to integration time, while the amplitude of the saturation responsivity effect is independent of integration mode. For warmer thermal link temperatures, the saturation dark offset effect magnitude becomes larger while saturation responsivity effect magnitude remains the same. The saturation responsivity effect is unaltered for saturation durations greater than 13 s and is less for saturation durations less than 46 ms. There are detector-to-detector variations in the magnitude of the saturation responsivity and dark offset effects that have peak-to-peak values approximately the same magnitude of the saturation effect.

Each array has its own saturation effect recovery time constant that is approximately the same value for the saturation dark offset and responsivity effects. This time constant is independent of saturation flux level and integration mode. However, the recovery time constant becomes shorter for higher thermal link temperatures, and is also decreased by stimulating the detectors.

Acknowledgments

This work was sponsored by the BMDO. The author gratefully acknowledges the support of BMDO and the MSX program.

References

1. J. Tansock, ''Saturation dark offset effect,'' Internal Space Dynamics Laboratory, Utah State University memorandum (1994).
2. ''SPIRIT III infrared sensor ground calibration report, Vol. 1 and 2,'' Space Dynamics Laboratory, Utah State University, SDL/94-053 (Oct. 1994).
3. ''SPIRIT III sensor user's guide, revision 5,'' Space Dynamics Laboratory, Utah State University, SDL/92-041 (1995).
4. ''SPIRIT III integrated ground and on-orbit calibration report in support of Convert 3.2, Vol. 1 and 2,'' Space Dynamics Laboratory, Utah State University, SDL/96-042 (Oct. 1996).

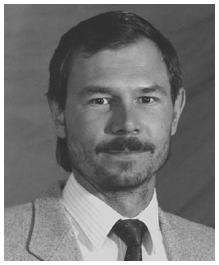

Joseph J. Tansock is a calibration engineer with the Space Dynamics Laboratory at Utah State University where he specializes in IR sensor calibration. He received a BS in physics and applied mathematics from Weber State University in 1988 and an MS in instrumentation physics from the University of Utah in 1992. Prior to 1992 Mr. Tansock was a flight equipment test and analysis engineer for Rockwell International. His research interests include IR imaging systems, calibration of complex IR sensors, and data analysis.